PERGAMON

Available online at www.sciencedirect.com

SCIENCE DIRECT®

Deep-Sea Research I 50 (2003) 1005–1021

DEEP-SEA RESEARCH
PART I

www.elsevier.com/locate/dsr

The influence of tidal hydrodynamic conditions on the generation of lee waves at the main sill of the Strait of Gibraltar

José J. Alonso del Rosario*, Miguel Bruno Mejías, Águeda Vázquez-López-Escobar

Applied Physics Department, Physical Oceanography, University of Cadiz, Polígono del Rio San Pedro s/n, Puerto Real, Cádiz, Spain

Received 16 July 2001; received in revised form 7 May 2003; accepted 15 May 2003

Abstract

The main sill of the Strait of Gibraltar (Camarinal Sill) is an area of very energetic internal wave activity. The highest amplitude internal wave is the well-known internal bore, generated at critical conditions over Camarinal Sill. A very energetic lee wave has recently been found and reported. This occurs in neap tides when favorable combination of the stratification, vertical profile of horizontal background velocity, and bottom topography determines its generation. When the lee wave is developed the manifestation of high-amplitude internal waves is observed at the sea surface as high-frequency chaotic oscillations, named *boiling waters*. We analyze the generation of the lee wave over the main sill of Gibraltar Strait on the basis of the data from a ship mounted ADCP, multi-probe CTD data taken during a survey carried out in November 1998, and the numerical solution of the Taylor–Goldstein equation for the prevailing hydraulic conditions previous to its generation. Stratification is computed from CTD data, and the tidal current prediction is made from the 2 years of ADCP hourly data at Camarinal Sill gathered during the Gibraltar Experiment 94-96. The main characteristic is that they happen during neap tides, and their magnitude is comparable to the internal bore generated during spring tides. The classical internal bore and the lee waves are different phenomena, and the presence of the latter is an indicator of minimum flow over Camarinal Sill. A prediction model for lee waves based on the tidal hydrodynamic conditions is also developed.

Keywords: Lee waves; Resonant processes; Strait of Gibraltar; ADCP

1. Introduction

Surface manifestations of internal motion related to the interaction of flows with topography are well-known oceanographic phenomena. They are manifested in slight modulations of the free surface, named *surface slicks*. The influence of more energetic waves is observed at the sea surface as chaotic motion and breaking of short waves. This usually results in bands of rectangular plumes aligned with the internal wave crests (La Violette and Lacombe, 1988; New and Pingree, 1992). Spanish fishermen call these surface signatures as *hervideros* in clear association with the behavior of

*Corresponding author.
E-mail address: josejuan.alonso@uca.es (J.J.Alonso del Rosario).

0967-0637/03/$ - see front matter
doi:10.1016/S0967-0637(03)00097-9

the surface water. The Spanish Navy gave the first references to them at the Gibraltar Strait and its surroundings in 1787 and in 1832 (Tofiño, 1832). The first non-Spanish reference was given by Purdy (1840) who called them *streamers*. They happen without previous signs and can be strong enough to make the steering of a ship difficult.

The Strait of Gibraltar is one of the oceanic regions with very intense internal wave activity where surface signatures are frequently observed. Many studies of such signatures have been carried out using different methods (Frassetto, 1964; Ziegenbein, 1969; Cavanie, 1972; La Violette, 1986; Richez, 1994; Bray et al., 1990; Watson and Robinson, 1990; Brandt et al., 1996). Most of the literature on internal waves in the Strait of Gibraltar has been focused on the internal tide or on the generation, propagation and release of the internal bore formed when the conditions are critical downstream of Camarinal Sill at maximum Mediterranean outflow. This differs from the phenomenon west of the sill with small amplitude westward travelling waves, which hardly produce a detectable surface signature. All of them are generated during spring tides.

There is another kind of internal wave, which appears only during neap tides. It has been reported in Lacombe and Richez (1984), La Violette and Lacombe (1988) and Richez (1994), but the only studies on its origins and effects are those of Bruno et al. (2002) and Echevarría et al. (2002). Such a structure has been identified as a very energetic internal lee wave related to resonant processes, and it occurs when the flow stops the propagation of the internal wave under subcritical flow conditions over Camarinal Sill. The hydrodynamic conditions needed for the generation of these waves at Camarinal will be investigated here to develop some criteria to predict the occurrence of this phenomenon. The main characteristic is that it happens during neap tides, and its magnitude is comparable to the internal bore generated during spring tides. Internal bore and lee waves seem to be incompatible phenomena (Bruno et al., 2002), as will be proved later in this paper.

The linear theory of hydrodynamic stability (Chandrasekar, 1981; Kundu, 1990; Gill, 1982) is applicable to the characterization of the most favorable and initial conditions for the occurrence of this kind of wave. According to Chandrasekar (1981) any flow is unconditionally unstable (small perturbations can grow infinitely). Hence instabilities must always arise, but it is possible to investigate which of them can be amplified under suitable environmental conditions (stratification and the background horizontal velocity profiles).

2. Observations and data processing

The survey was carried out in November 1998 on the R/V *El Investigador*. Observations were made with a ship-mounted ADCP used to control drilling operations at Camarinal Sill. Drilling always took place during neap tides, when currents were weaker, hence all our results are unavoidably related to these conditions. The velocity field $[u,v,w]$ was obtained from the ADCP data. The sampling period was one minute and the vertical resolution was 10 m. The data from a multi-parameter probe carrying CTD-probe with nephelometer are also available. The area under study is shown in Fig. 1. When a boiling water structure was detected (times given in Table 1) the ship crossed it longitudinally while observations were made.

In order to analyze the ADCP records, the horizontal velocity u at a depth of 20 m was evaluated and plotted (Fig. 2) to see when the horizontal velocity gradient, responsible for the chaotic motion at the sea surface, was maximal. This allowed us to distinguish four checkpoints to validate the methodology developed later in this paper. These moments can be observed in the high-frequency oscillations during outflowing currents on November 24–27, 1998. Once the occurrence times were known, the longest runs were selected and the velocity field was calculated from the raw data at depths from 20 to 255 m following the quality control of the data. The high-frequency waves were filtered by FFT with cut off frequency corresponding to 5 min if the run was short. If the run was long enough, a 15-min filtering was used. Tidal periods were not removed.

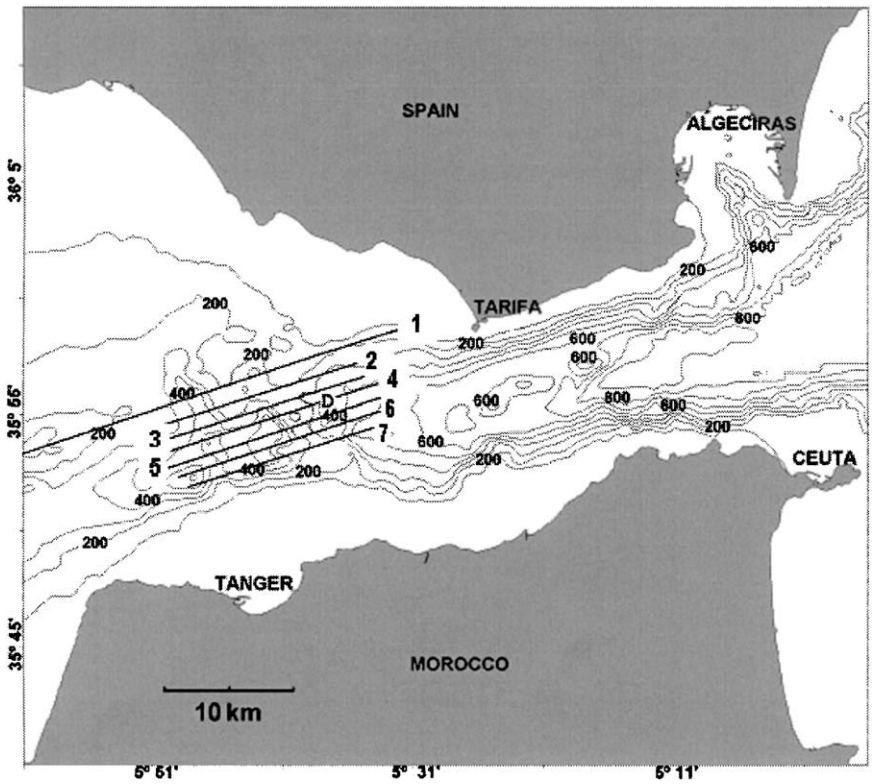

Fig. 1. Map of the Strait of Gibraltar. The bottom topographic profiles are numbered 1–7. They crossed Camarinal Sill. *D* indicates the location of the ADCP that was moored during the Gibraltar Experiment 94-96.

Table 1
Time periods (GMT) when the boiling water structures were recorded

Date	Hours	Main observed wavelengths (m)
24/11/98	13:00–17:30	1250,909,833,714,588,556
27/11/98	16:30–19:00	1250,1000,588,500
28/11/98	11:00–13:00	2500,1667,625,588,476

The November 28 and November 29, 1998, events are not shown here but they were observed.

The wavelengths of the different internal events (Table 1) were computed by maximum entropy spectral analysis (MESA), using Burg's approach (Marple, 1987; Alonso et al., 1994), of the vertical velocity field at a depth of 45 m.

The processed and filtered vertical velocity field for the event of November 28, 1998, 13:30 h is shown in Fig. 3. A typical structure of an internal wave can be observed at the depth of the interface (150 m) as upward and downward movements at left and right sides, respectively, of the zero vertical velocity line.

3. Initial perturbation and a conceptual framework

The generation of lee waves depends on the background velocity profile and on the stratification conditions. Hydrodynamic perturbation grows infinitely under favorable conditions. We shall analyze which type of instability is the responsible for triggering the process. One can see in the experimental data that the depth of the interface is far from the bottom. Hence the initial perturbation is induced by the interaction between two layers with relative motion. The dispersion relationship for the Kelvin–Helmholtz instability

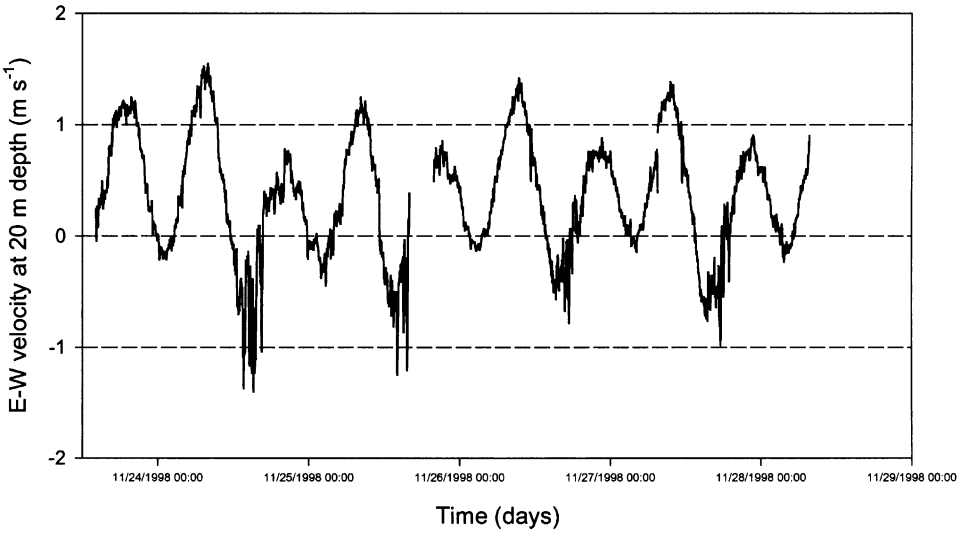

Fig. 2. U component of the velocity at 20 m depth. Time index in days.

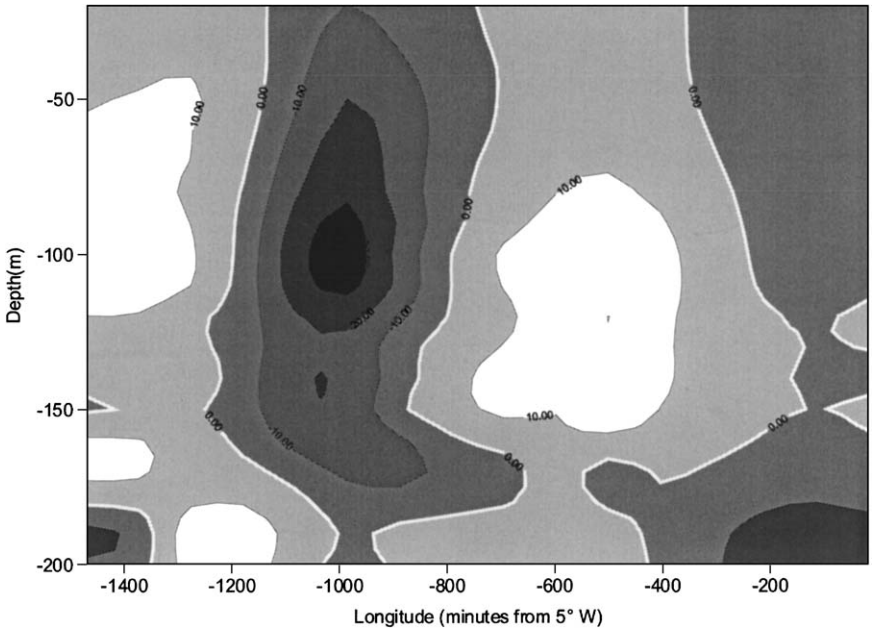

Fig. 3. Observed vertical velocity field for the same period as in Fig. 2.

(Kundu, 1990) is written as

$$c = \frac{u_1\rho_1 + u_2\rho_2}{\rho_1 + \rho_2} \pm \sqrt{\frac{g}{k}\frac{\rho_2 - \rho_1}{\rho_1 + \rho_2} - \rho_1\rho_2\left(\frac{u_1 - u_2}{\rho_1 + \rho_2}\right)^2},$$

where u_i and ρ_i are the velocities and densities of the two layers, g is the acceleration due to gravity, k is the wave number and c is the phase speed of the perturbation. This expression gives the velocity of the Kelvin–Helmholtz wave perturbation in

terms of the wavelength, the density of the two layers and their relative velocities. Notice that it is not a function of the thickness of the layers. Although this kind of instability can arise for any difference of velocities between the layers (Chandrasekar, 1981), the infinite growth of the perturbation occurs when the argument of the square root is negative; therefore is not strictly the Kelvin–Helmholtz instability. Let us investigate whether this type of instability produces the initial perturbation for the lee wave under study. We assume the following values for one of the observed events: $U_1 = -0.74$ m/s, $U_2 = -1.46$ m/s, $\rho_1 = 1027.3$ kg/m^3, $\rho_2 = 1029.9$ kg/m^3, $h_1 = 90$ m, $h_2 = 160$ m. The observed wavelength is 1000 m. The exponential growth is observed when $\Delta u >$ 2.81 m/s. In our case the velocity difference is 0.72 m/s, smaller than the computed limit. It is our opinion that the driving force of the lee waves in neap tides is not the interaction between the layers because the conditions for the Kelvin–Helmholtz instability are absent.

Now we can introduce a simple conceptual model. When an oscillatory (tidal) and unperturbed current flows over bottom topography in a stratified fluid, many kinds of hydrodynamic perturbation arise, which distort all the fields. From the previous discussion the interaction of the flow with the topography must be the driving process. Any kind of perturbation between the existing layers can be neglected. A perturbation is generated in the lower part of the deepest layer. If the conditions for its upward propagation are favorable, it can propagate to the interface and perturb it. This perturbation will propagate in the direction opposite to the flow. When the relative wave speed is zero (c=0), the internal wave is arrested by the flow (Bogucki et al., 1999) and a feedback mechanism is initiated. Energy is radiated from the bottom and reflected from the surface. Both energy fluxes superimpose. This superposition will produce an amplified wave that will reach the surface producing the surface slicks, leading to the dissipation of energy while the input of energy from the bottom is continuous. This is necessary for the maintenance of the phenomenon. If the perturbation, produced by the interaction of the background velocity with the bottom, has a wavelength close to one of the resonant wavelengths, and if the conditions are suitable, then the amplification takes place and the process we analyze is triggered.

Some basic calculations are needed to clarify the suggested scheme for the propagation of internal perturbation. We assume a simplified buoyancy profile by dividing the whole column into three layers (from CTD data) with the following buoyancy frequencies: $N_1 = 4.4\text{E-}3\ \text{s}^{-1}$, $N_2 = 2.76\text{E-}2\ \text{s}^{-1}$ and $N_3 = 9.78\text{E-}3\ \text{s}^{-1}$ (subscript 1 denotes the lower 100 m layer, subscript 2 denotes the interface 20 m thick and subscript 3 denotes the upper 100 m thick layer). We assume that the horizontal wavelength of the observed event is 1000 m, the frequency is $\omega = kU = 2\pi/1000 \times 0.8 = 1.675\text{-}2$ rad/s, where U is the average velocity of the lower layer. The frequency is constant in the whole column. Following Gill (1982) and Konyaev and Sabinin (1992), the dispersion relationship for internal waves in polar coordinates in a continuously stratified medium is written as

$$\omega = N \cos(\alpha),$$

where α is the absolute value of the angle with respect to the horizontal bottom. When rotation is taken into account we get

$$\frac{\omega^2 - f^2}{N^2 - f^2} = \cos^2(\alpha).$$

Computation with both expressions was carried out and the results did not differ greatly. Hence the earth's rotation is not important in the generation and vertical propagation of this kind of internal

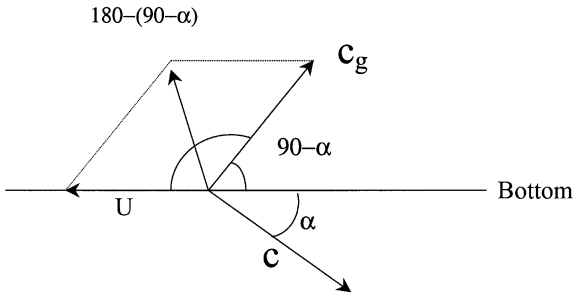

Fig. 4. Scheme of angles for the computation of the direction of the celerity group (following Garrett and Munk, 1972).

wave. We calculated the following angles for the celerity from the dispersion relation: $\alpha_1 = 30.2^\circ$, $\alpha_2 = 79.5^\circ$ and $\alpha_3 = 59.0^\circ$. After the correction of these results (Fig. 4) following Garrett and Munk (1972), the angles for the celerity group are $\alpha'_1 = 120.18^\circ$, $\alpha'_2 = 169.50^\circ$ and $\alpha'_3 = 149.00^\circ$. It follows from the angle calculations that the energy propagates upward in an almost normal direction to the bottom. Some remarks should be made. Notice that for the lower layer $\omega = Uk > N_1$; hence there is no harmonic solution, and the wave propagates vertically and is exponentially damped. However, the driving force of the process is so strong that perturbations reach the intermediate layer. Here the conditions for the upward propagation are favorable ($\omega = Uk < N_2$ and $\omega = Uk > N_3$), which leads to a harmonic solution.

The conditions for the upward propagation of the perturbation in the lower layer are not favorable, but since the perturbation is strong it reaches the intermediate layer, where the conditions are more favorable for the perturbation, which therefore reaches the sea surface. In the next section we shall use two approaches to evaluate the wavelengths of the perturbations, which propagate in the water column.

4. Theoretical background

4.1. Resonant wavelength derived on the basis of a two-layer flow model

Lee waves occur when suitable stratification and currents make the phase speed of the generated waves close to zero (Bogucki et al., 1999). The phase speed is a function of the dynamical and stratification conditions in the water column. The first simple approach to study what wavelengths may become resonant under given hydraulic conditions is made on the basis of the two layer dispersion relationship.

The two-layer dispersion relationship for interfacial waves in the non-hydrostatic case can be expressed as (Farmer and Armi, 1999)

$$c(k) = \frac{U_1 R_1 + U_2 R_2}{R_1 + R_2} \pm \frac{\sqrt{k^2(U_1 R_1 + U_2 R_2)^2 + k^2(R_1 + R_2)(U_1^2 R_1 + U_2^2 R_2) - \rho_2 g' k}}{k(R_1 + R_2)}, \quad (1)$$

where U_i is the velocity of the layer (i=1,2), $R_i = \rho_i \coth(k \cdot h_i)$, h_i is the thickness, ρ_i is the density and g' is the reduced gravity defined as $g' = g(\rho_2 - \rho_1)/\rho_2$, where g is the gravity. Finally $c(k)$ is the phase speed of the interfacial wave as a function of the wave number k=$(2\pi)/L$, where L is the wavelength of the interfacial wave. Subscript 1 refers to the upper layer and 2 to the deeper one.

From Eq. (1) it is possible to obtain the dispersion relationship for several hydraulic conditions. The dispersion relationship for the values given in Section 3 is shown in Fig. 5. We are interested in the wavelength with null relative velocity (c=0). It is clear that waves with a wavelength greater than 800 m can propagate against the flow (phase speed greater than zero). Waves with negative phase speed propagate out of the Camarinal Sill area because of the advection by the flow. Only waves with zero phase speed relative to the bottom can became resonant. The observed horizontal wavelength of the most

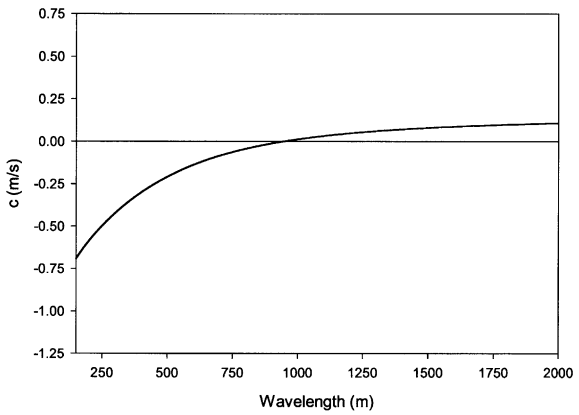

Fig. 5. Two-layer dispersion relationship for the conditions specified in the text. Positive values refer to eastward travelling waves. Wave numbers have been translated into wavelengths.

pronounced internal wave was about 1000 m (Bruno et al., 2002). Hence, we can obtain a good approximation of the same wavelength from the dispersion relationship.

The densimetric or internal Froude number is defined as

$$G^2 = \sum_{i=1,2} \frac{u_i^2}{g' h_i}.$$

When $G^2 > 1$ the flow is supercritical, when $G^2 < 1$ the flow is subcritical, and when $G^2 = 1$ the flow is critical. For critical and supercritical conditions on the main sill, the flow is hydraulically controlled and internal waves cannot travel against the flow. When the flow is critical on the sill the internal lee waves can be generated leeward as the well-known internal bore in the Gibraltar Strait. If the flow is subcritical, no internal waves can exist in the hydraulic sense. For the above values $G^2 = 0.784$; this is a subcritical flow, which has nothing to do with the classical internal bore observed in the Strait of Gibraltar (Armi and Farmer, 1988; Richez, 1994).

Stratification is very important in the analysis of the dispersion relationship. It is known that sometimes the vertical structure of the water column in the Strait of Gibraltar corresponds to a three-layer structure, or even to a one layer when the mixing is strong, instead of the typical two-layer structure. If a continuous stratification is allowed for given hydraulic conditions, more than one wave can exist, but the two-layer dispersion relationship will predict only one wavelength. Nevertheless, the two-layer dispersion relationship is a very useful preliminary approach.

4.2. Resonant wavelength in continuously stratified flows

The Navier–Stokes equations for a linear continuously stratified flow with no rotation, with Boussinesq condition and 2D with x-axis positive eastward and z-axis positive upward with the origin at a flat bottom are (Kundu, 1990):

$$\frac{\partial u}{\partial t} + u\frac{\partial u}{\partial x} + w\frac{\partial u}{\partial z} = -\frac{1}{\rho_0}\frac{\partial p}{\partial x},$$

$$\frac{\partial w}{\partial t} + u\frac{\partial w}{\partial x} + w\frac{\partial w}{\partial z} = -\frac{1}{\rho_0}\frac{\partial p}{\partial z} - \frac{g}{\rho_0}\rho,$$

$$\frac{\partial \rho}{\partial t} + u\frac{\partial \rho}{\partial x} + w\frac{\partial \rho}{\partial z} = 0,$$

$$\frac{\partial u}{\partial x} + \frac{\partial w}{\partial z} = 0,$$

where $[u(x,z,t),\ w(x,z,t)]$ is the velocity field, $p(x,z,t)$ is the pressure field and $\rho(x,z,t)$ is density. Now decomposing the velocity, pressure and density into the sum of an unperturbed or background term and a perturbed one, omitting the non linear terms (Chandrasekar, 1981), subtracting the basic state, introducing the stream function and applying normal modes, after some algebraic transformations it is easy to obtain a single equation in terms of the complex amplitude of the stream function $\hat{\psi}(z)$:

$$\hat{\psi}_{zz} + q(z)\hat{\psi} = k^2\hat{\psi}, \tag{2}$$

where the potential function is

$$q(z) = \frac{N^2}{(U-c)^2} - \frac{U_{zz}}{(U-c)} \tag{3}$$

and where $\hat{\psi}(z)$ is the complex amplitude of the stream function, $U(z)$ is the background horizontal velocity, $N^2(z)$ is the buoyancy frequency and c is the phase speed of the internal wave. Expression (2) is known as the *Taylor–Goldstein equation* (Kundu, 1990; Konyaev and Sabinin, 1992), and it plays an important role in the study of hydrodynamic instability. Subscripts indicate derivatives. Eq. (2), together with the non-slip boundary conditions $\hat{\psi}(0) = \hat{\psi}(h) = 0$, is a Sturmian problem where the solutions are the eigenvectors, $\hat{\psi}_n$, with their correspondent eigenvalues, k_n^2. The eigenvectors satisfy the orthogonality condition:

$$\int_0^h \hat{\psi}_n(z)\hat{\psi}_m(z)\,\mathrm{d}z = \delta_{nm},$$

where δ_{nm} is the Kronecker symbol.

For an arbitrary buoyancy frequency, $N(z)$, and a horizontal velocity profile of the background $U(z)$, (i.e. for an arbitrary $q(z)$ function) Eq. (2) must be solved numerically. Several numerical methods have been used. We are interested in the

internal waves that can be resonant, which is the equivalent to the arrested waves. Hence in Eq. (3) a zero relative phase velocity, c=0, is chosen (Bogucki et al., 1999; Bruno et al., 2002).

In addition, there is not a unique solution to Eq. (2). However, there is a method to determine the wavelength from the solution of the Sturmian problem. In the next section, it will be shown that the wavelengths must be close to the typical scales of topographical variability. For that reason it is necessary to analyze carefully the bottom topographic sections.

4.3. Bottom topography length scales

In order to compute the typical scales of topographic wavelengths, which can influence the flow-topography interaction, we used the seven bottom topography profiles shown by straight lines in Fig. 1. We performed the spectral analysis of the topography sections with MESA Burg's algorithm (Marple, 1987; Alonso et al., 1994). The MESA procedure was chosen instead of FFT because of the problems with the latter when a small data series is used. Sections 4 and 6 and their MESA spectra in dB are shown in Fig. 6. The wavelengths from these analyses are presented in Table 2. These values are very useful in deciding whether to accept or reject the computed resonant wavelengths. This can be named a *topographic criterion of existence* for the internal lee waves in the sense that only the wavelengths found in the topography will be enhanced if a suitable combination of flow and stratification is reached. Other waves with lower and higher wave numbers will not be considered.

From this analysis it is possible to find different wavelengths depending on the bottom section chosen for the analysis. Wavelengths over 1000 m are found in profiles 1, 2 and 7. In profiles 3 to 6 the wavelengths are shorter, 500–800 m. This is in very good agreement with the observations of Richez (1994). She found that north and southward of the sill the wavelengths were greater than those detected on the sill. From the experimental data it was found that the most probable wavelength is about 1000 m, in profiles 3–7. This is also in very good agreement with the results shown in Section 6.

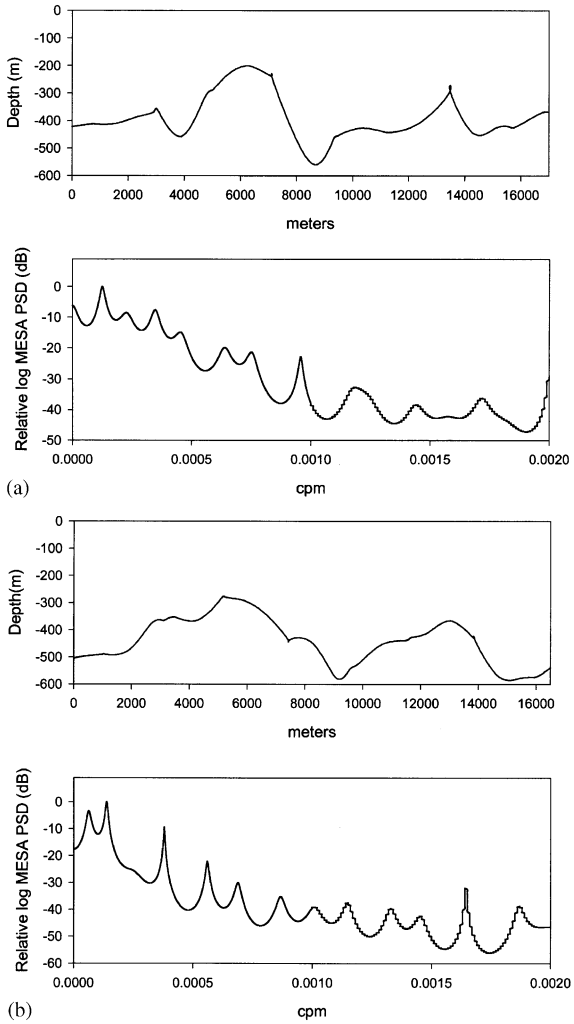

Fig. 6. (a) Bottom topographic profile 3 and its MESA spectrum. (b) Bottom topographic Section 4 and its MESA spectrum. For the bottom topographic profiles the horizontal scale is in meters starting from the most eastern point, vertical scale for spectra is in dB.

5. Numerical experiments

Several combinations of incoming flows and stratification conditions using the continuously stratified flow approach of Section 4.2 will be

Table 2
Significant wavelengths from maximum entropy spectral analysis of topographic profiles

Profile	Wavelengths found in the bottom topography (m)
1	999,666,454
2	1110,624,454
3	833,526,416
4	588
5	434
6	624
7	1110,624,454

Only wavelengths longer than 400 m are given in the table.

investigated. The computation of the parameterization of the incoming velocity and stratification will be detailed in Sections 5.1 and 5.2. Several cases assuming the depth of the interface as the depth of maximum shear and maximum buoyancy will be analyzed. In other cases, it is assumed that the maximal exchange and the interface are located 20 m above the maximum shear depth following Bryden (2000) and CANIGO (1999). In addition these two similar cases are analyzed considering an additional barotropic flow. This set of experiments will shed light on the characteristics of the generated lee waves at different hydrodynamic situations.

The numerical experiments have three main objectives. The first is the computation of the vertical profiles of horizontal velocity, the second is the computation of the associated buoyancy frequency profiles and the third is the numerical solution of Eq. (2) for several cases.

5.1. Computation of horizontal velocity profiles

Two years of hourly data records from an Acoustic Doppler Current Profiler (ADCP) moored at Camarinal Sill during the Gibraltar 94-96 experiment (Fig. 1) were used. The time spans covered in each phase of the experiment are presented in Table 3. The depth interval of the analyzed data was 10 m, and the layer close to the surface was not considered because of the reflections of acoustic beams. The harmonic constants for each depth were obtained by least-squares harmonic analysis (Foreman, 1998) for the full

Table 3
Start time and duration in hours of the four phases of the ADCP data records in the Gibraltar Experiment 94-96

Start time	Number of records in the series
15:00 h 21/10/1994	3954
18:45 h 06/04/1995	4554
13:15 h 16/10/1995	4494
11:15 h 21/04/1996	3739

period. Amplitudes and Greenwich phase lags for M2, S2, K1 and O1 tidal waves are presented in Table 4.

The full set of harmonic constants was used to perform hourly predictions of the tidal current in November 1998 at all depths. However, the analysis was focused on the periods of outflowing (see Table 1). The interest in such periods arises from the fact that this is the time when the internal lee waves, or boiling water structures, were detected and registered at Camarinal Sill (Bruno et al., 2002).

After harmonic prediction an analytical function was fitted to the hourly vertical profiles of horizontal velocities in order to: (a) improve the vertical resolution and provide smoothed velocity profiles to ensure the numerical stability of the scheme of resolution for Eq. (2), and (b) to obtain an initial approximation of the depth of the interface from the maximum shear depth. After some trial and error, we found that the best was a five-parameter sigmoidal function:

$$U(z) = U_0 + \frac{U_a}{\left(1 + \exp\left(-(z - U_{z_0})/U_b\right)\right)^{U_c}}, \qquad (4)$$

where z is the depth, U_0 denotes the value of the velocity at the sea surface, U_a is the amplitude or range of the profile of horizontal velocities, U_b is the thickness of the interface layer, U_{z0} denotes the depth of maximum shear and U_c is a free parameter.

The fitting of the velocity data to Eq. (4) is clearly nonlinear. Because of this a Levenberg–Marquardt algorithm was used (Press et al., 1986). All the fits had a correlation coefficient better than $r^2 = 0.98$ (Fig. 7). The deviations between the predicted vertical profile of tidal current

Table 4
Harmonic constants of the along Strait component

Depth	$O1$	$K1$	$M2$	$S2$
45	0.2945(356.04)	0.2725(70.40)	1.0423(139.00)	0.4223(172.80)
55	0.2948(356.12)	0.2745(70.19)	1.0505(139.17)	0.4254(173.14)
65	0.2936(356.61)	0.2743(70.34)	1.0560(139.70)	0.4276(173.64)
75	0.2908(357.97)	0.2708(70.92)	1.0588(140.63)	0.4263(173.98)
85	0.3039(353.78)	0.2713(67.86)	1.1412(139.34)	0.4411(174.55)
95	0.2772(1.96)	0.2583(73.81)	1.0451(143.61)	0.4146(174.71)
105	0.2695(3.91)	0.2516(75.73)	1.0296(145.43)	0.4072(175.11)
115	0.2606(5.59)	0.2454(77.80)	1.0104(147.34)	0.4003(175.47)
125	0.2511(7.02)	0.2392(79.93)	0.9905(149.15)	0.3933(175.43)
135	0.2414(7.77)	0.2345(82.32)	0.9764(150.71)	0.3846(175.14)
145	0.2313(8.92)	0.2304(84.99)	0.9736(151.63)	0.3753(174.48)
155	0.2221(10.49)	0.2282(88.32)	0.9808(151.83)	0.3647(173.29)
165	0.2152(13.27)	0.2252(92.77)	0.9969(151.21)	0.3483(171.60)
175	0.2113(17.21)	0.2227(97.58)	1.0158(149.97)	0.3280(168.45)
185	0.2119(21.64)	0.2202(102.10)	1.0317(148.18)	0.3039(163.56)
195	0.2146(25.82)	0.2156(105.84)	1.0373(145.67)	0.2829(157.49)
205	0.2193(28.89)	0.2117(108.70)	1.0271(142.48)	0.2681(151.80)
215	0.2247(30.72)	0.2104(109.95)	1.0001(138.51)	0.2647(147.87)
225	0.2258(31.08)	0.2098(110.37)	0.9624(133.94)	0.2640(145.55)
235	0.2177(30.70)	0.2048(109.63)	0.9228(129.11)	0.2608(143.94)
245	0.2023(29.90)	0.1933(109.58)	0.8862(124.71)	0.2534(141.37)
255	0.1863(29.20)	0.1768(109.71)	0.8494(121.01)	0.2444(137.82)

Velocities are in m/s and Greenwich phase lags, between parentheses, are in degrees.

and the parametrization from Eq. (4) are quite small in all the cases, showing the correctness of the fits.

There are several criteria for the depth of the interface in the Strait of Gibraltar. The most common is to use the depth of the 37.5 isohaline. In Bruno et al. (2000) the depth of the maximum shear was successfully used as an estimate of the depth of the interface, similar to the analysis of Bryden (2000). The value of the U_{z0} parameter is considered as the first approximation for the depth of the interface, and it will be used in this way in the next sections with some considerations that depend on the analyzed case.

5.2. Buoyancy frequency profiles

The buoyancy profile is computed from the density profile (Bruno et al., 2002). Since the survey was carried out during neap tides, the density and the buoyancy profiles represent only this tidal stage. The density profile has an almost constant vertical structure that can be described in terms of Eq. (4) as

$$\rho(z) = r_0 + \frac{r_a}{\left(1 + \exp\left(-(z - r_{z_0})/r_b\right)\right)^{r_c}}. \tag{5}$$

Eq. (5) is used for the computation of the density profile. The mean computed parameters are $r_a = 3.36$, $r_b = -10.08$, $r_c = 1.29$ and $r_0 = 1026.5$, and the depth of the interface was taken from the results of the fits of the five parameter sigmoidal function on the tidal current prediction assuming that the maximum of $N^2(z)$ is located near the shear maximum. r_{z0} is considered an estimate of the interface depth, where the maximum buoyancy is located. Once an analytical expression of the density profile is given, the computation of the buoyancy frequency function is straightforward.

5.3. Numerical computation of the resonant wavelengths

The numerical solution of Eq. (2) can be found with standard software packages after taking the

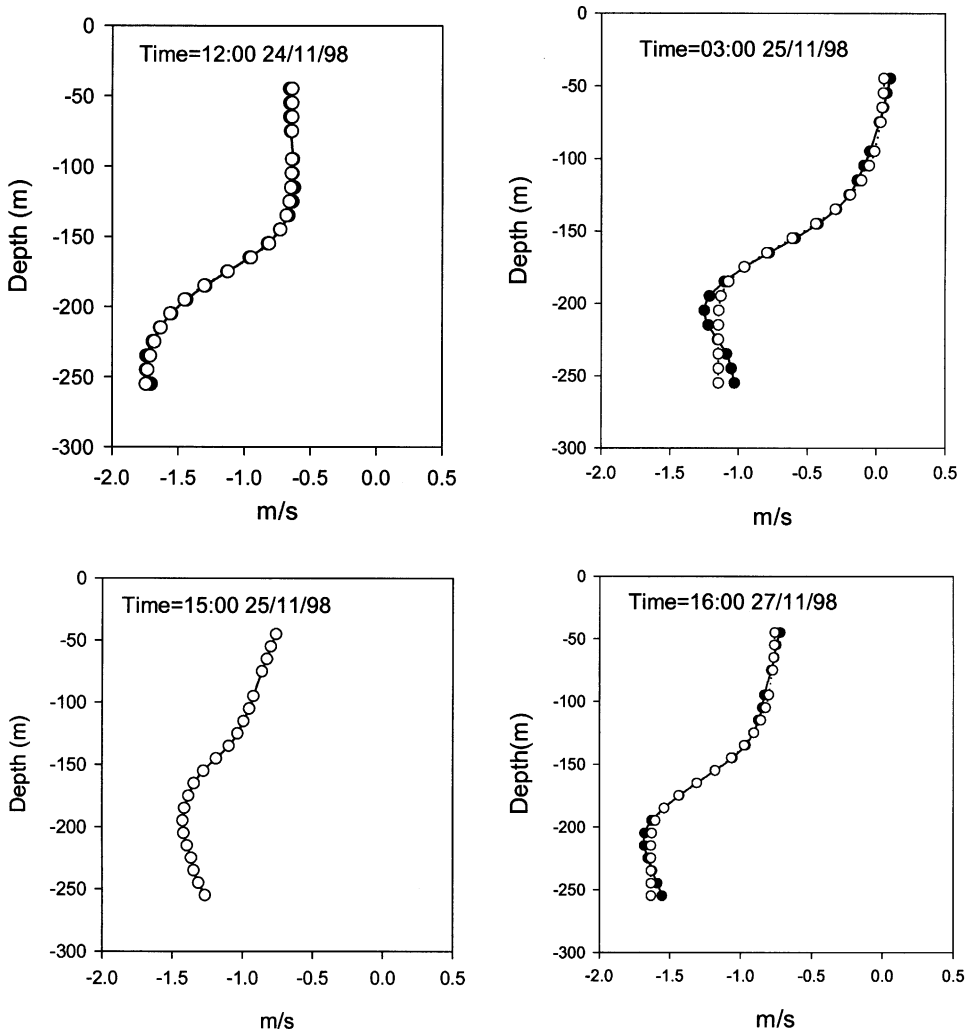

Fig. 7. Fitting of Eq. (4) on the profile of horizontal velocity for different time moments.

complex conjugate of Eq. (2) (Kundu, 1990) or following the method detailed in Henrici (1962). The latter consists of the formulation in terms of finite differences of Eq. (2) in the domain under study and the solving of the resulting eigenproblem. It has infinite solutions, but only a few of them will be physically possible. These are called *stable oscillation modes*. The others are associated with unstable flow structures and are not analyzed. Using eigenvalues k^2 one can calculate the correspondent wavelength of the associated eigenvectors. In order to obtain justified results and escape numerical rounding errors, all estimates were recalculated with different sampling (Sacks, 2001, pers. comm.). The comparison yielded excellent results. In addition the SLEIGN program (Bailey et al., 1991) was used in order to verify the results.

Once the Sturmian problem is solved, the perturbed velocity and density amplitudes can be computed by:

$$\hat{\rho}_n(z) = -C\,\frac{\rho_0 N^2}{gU}\hat{\psi}_n, \tag{6a}$$

$$\hat{u}_n(z) = C\,\frac{\partial\hat{\psi}_n(z)}{\partial z}, \tag{6b}$$

$$\hat{w}_n(z) = -\mathrm{i}Ck\hat{\psi}_n(z) \tag{6c}$$

where C is an arbitrary constant that must be fitted and is equal to the observed amplitude of the oscillations. The velocity and density fields for the perturbed and steady states are:

$$\rho_n(x,z) = \hat{\rho}_n(z)\cos(kx), \tag{7a}$$

$$u_n(x,z) = \hat{u}_n(z)\cos(kx), \tag{7b}$$

$$w_n(x,z) = \mathrm{i}\hat{w}_n(z)\sin(kx). \tag{7c}$$

Therefore all the fields can be reconstructed. In Fig. 3 the measured vertical velocity field is shown. Notice the high-frequency phenomena. It is possible to build the theoretical field from Eqs. (6) and (7) following Bruno et al. (2002). The most energetic oscillation mode reproducing the main pattern of the field was considered. If higher frequency modes were considered, the noise increased, which made the results closer to the observed fields. The theory is unable to reproduce the behavior of the lower layer, where another circulation pattern is observed; however, this can be caused by to the superposition of oscillation modes with upward and downward propagation after total or partial reflection.

6. Results and discussion of the numerical experiments

In Section 4 we discussed some numerical experiments based on the Taylor–Goldstein equation. Two cases were considered, both during the outflow current. Each one has two sub-cases. In the first the depth of the interface is assumed as the depth of the maximum shear; in the second it was taken 20 m above the interface (Bryden, 2000) to simulate the maximal water mass exchange. In the first we considered a pure tidal flow (without long period waves). A resonant wave is generated when a pure tidal flow interacts with the topography. In the second case a steady barotropic tidal current of 0.20 m/s (westward and eastward) was added to the vertical profile of horizontal velocity (similar to the first case) to study the influence of a net flux when it generates the internal lee waves. This gives the best simulation of the real situation at the main sill of the Strait of Gibraltar. This is also the most complicated case. Since there are records only for November 24, 25, 27 and 29, 1998, the outflow was analyzed only for those days.

6.1. Case 1: the pure tidal flow

6.1.1. Case 1a: the case when there is no maximal exchange

We chose the same depth of the interface and maximum gradient of horizontal velocity. The resonant wavelengths computed from Eq. (2) are shown in Fig. 8a. Fig. 8b shows the tidal current prediction at a depth of 45 m depth on the basis of the harmonic constants given in Table 4. Finally, Fig. 8c shows the densimetric Froude number, G^2, for the same moments. In many cases the resonant wavelengths were not obtained in the solution of the Sturmian problem, because no resonant wavelengths could be found for the prescribed conditions given by the stratification and horizontal velocity profile. When the resonant wavelengths were calculated for other time than neap tides, the Sturm–Liouville problem had no solutions.

One can see from Fig. 8 that long resonant waves appear when the outflow velocity in the Mediterranean layer is greater than 1 m/s. This is the case for the November 24, 25 and 28 events. When the outflow velocity is higher than the *critical speed* of 0.5 m/s, the generated wavelengths are shorter than 850 m. However, when the outflow velocity becomes greater than the critical speed, the computed resonant wavelength is longer, and it can be as high as 2000 m. It must be noted that the events occur within the time period between 3 h before and 3 h after the maximum outflow velocity. In addition, the events never happen at the times of maximum speed, but always before or after, when the velocity is around 0.5 m/s. This is in very good agreement with the observations (Fig. 2a).

Several resonant waves can exist at a given condition, because the Sturm–Liouville problem does not have an unique solution. In this case there is a principal stable oscillation mode and several additional ones. The first determines the main

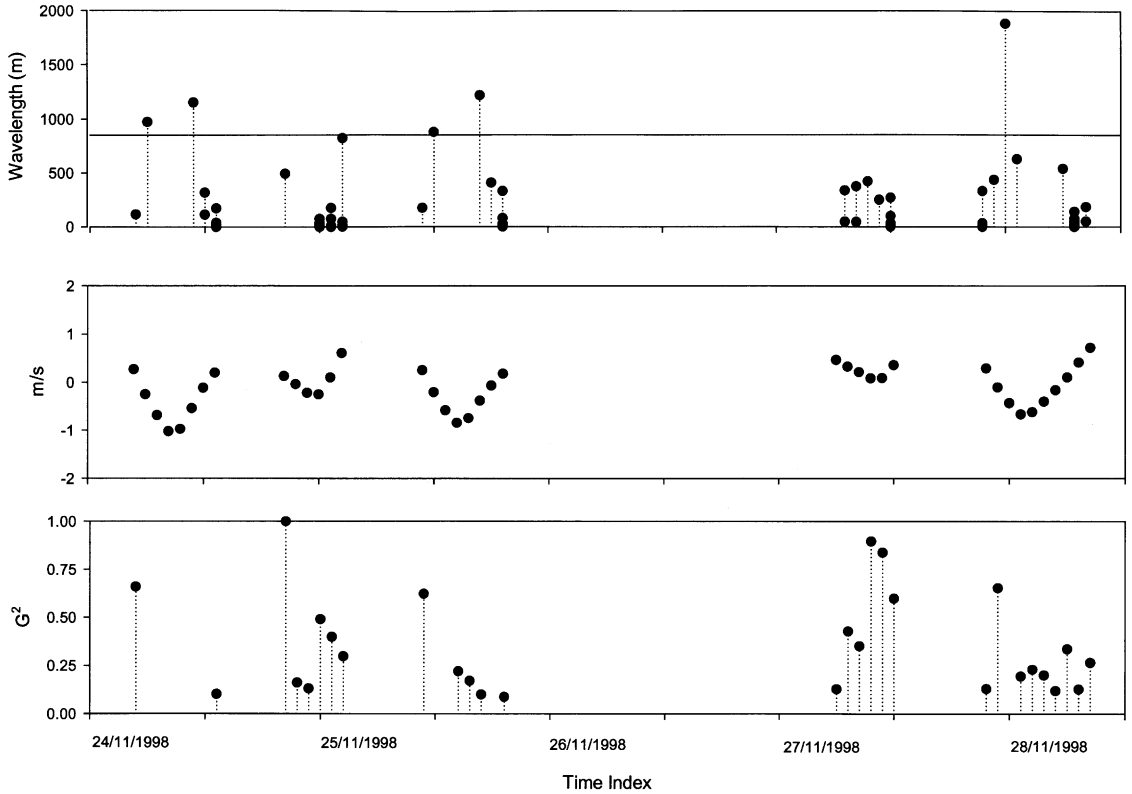

Fig. 8. Solutions for Case 1a: (a) resonant wavelengths; (b) tidal current prediction at 45 m depth; (c) associated densimetric Froude numbers. Dates from 07:00h 24/11/1998 to 01:00h 28/11/1998.

structure of the fields, and the others form the fine structure of the phenomenon. All of them must comply with the topographic criterion of existence proposed in Section 4.3.

The densimetric Froude number for the longer resonant wavelengths ranges from 0.75 to almost 1. Since G^2 is less than 1 the flow is subcritical, and no internal waves are observed, as described; but in our case the hydraulics constrain the existence of resonant waves only if G^2 is greater than 1.

It is very interesting to compare the calculated with the observed wavelengths (Table 1). For the structure detected on November 24, 1998, the wavelengths are slightly greater than 1000 m; for the event on November 27, 1998, the wavelengths are slightly greater than 650 m; and for the last event the wavelength is greater than 2000 m. However there is no 2000 m wavelength in the computation of the topographic wavelengths, which could be due to a poor choice of the bottom profile.

6.1.2. Case 1b: the case of maximal exchange

A similar experiment at the time of maximal water mass exchange between the Mediterranean and the Atlantic was carried out, taking into account Bryden's criterion (Bryden, 2000; CANIGO, 1999) for selecting the interface depth (where the maximum of the buoyancy frequency profile is found) 20 m above the depth of the maximum horizontal velocity gradient. The results are plotted in Fig. 9 except for the cases when $G^2 > 1$.

In this case most of the internal resonant activity is inhibited. Some resonant wavelengths are still

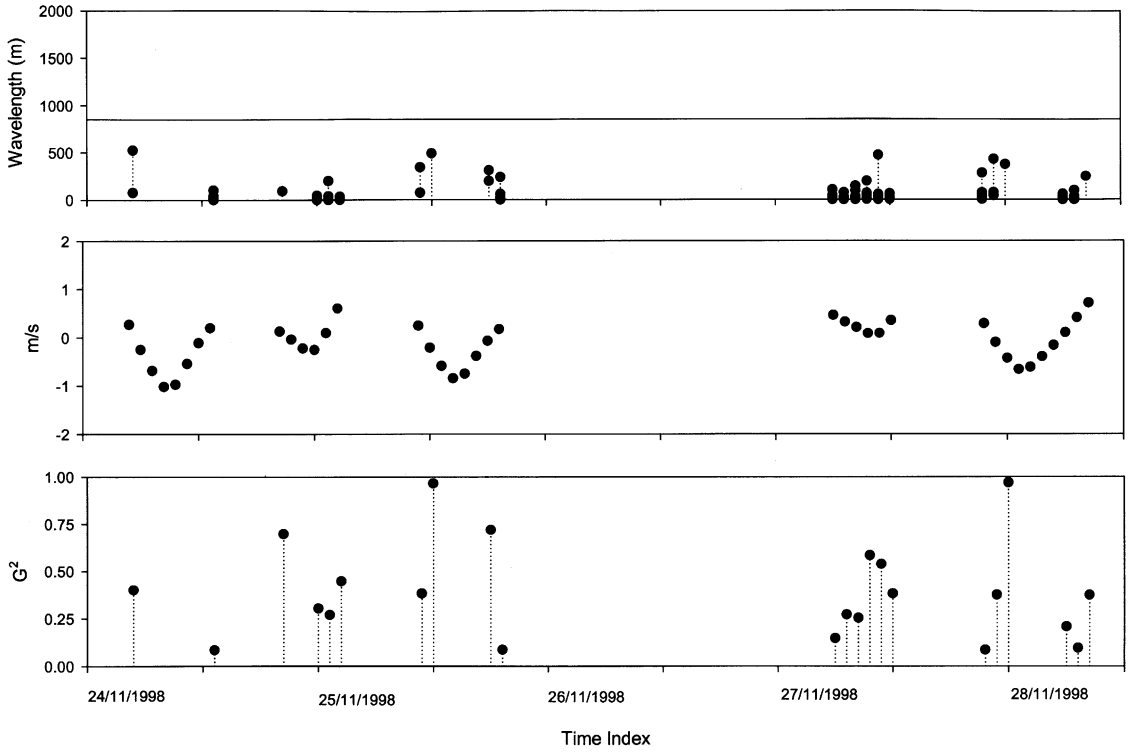

Fig. 9. Solutions for Case 1b: (a) resonant wavelengths; (b) tidal current prediction at 45 m depth; (c) associated densimetric Froude numbers. Dates from 07:00h 24/11/1998 to 01:00h 28/11/1998.

present but they are much shorter than before. Only at two time moments were the computed resonant wavelengths greater than 850 m: on November 25 and 28. Both occurred in the second outflow of the corresponding tidal cycle when the critical speed was exceeded. On the same day we found waves with wavelength about 750 m. In the two principal events the densimetric Froude number was close to 1. This is quite reasonable and corresponds to the assumption of maximal exchange. In addition none of the computed wavelengths coincide with those observed or computed from the topography wavelengths (Tables 1 and 2). This reinforces the assumption that maximal exchange inhibits the occurrence of lee waves. We conclude that this kind of lee waves occur only when water exchange does not reach its maximum, and during the maximum water exchange no lee waves are observed.

6.2. Case 2: experiments when barotropic current are included in the calculations

6.2.1. Case 2a: the case when there is no maximal exchange

Now we will investigate the consequences of a barotropic current on the generation of lee waves. A typical value of subinertial current of 0.20 m/s (Bryden et al., 1994) was added to the currents at all depths. The tidal current prediction was the same as in case 1a. The results of this experiment are shown in Figs. 10a and b. In both cases the conditions were the same as in case 1a, except for the addition of a current of −0.20 m/s in Fig. 10a and 0.20 m/s in Fig. 10b.

The internal resonant activity became higher and resonant wavelengths increased. The longest increased from 1000 to 2000 m (Fig. 10a). More waves appeared in the spectrum with wavelengths closer to 1000 m, even during the November 27,

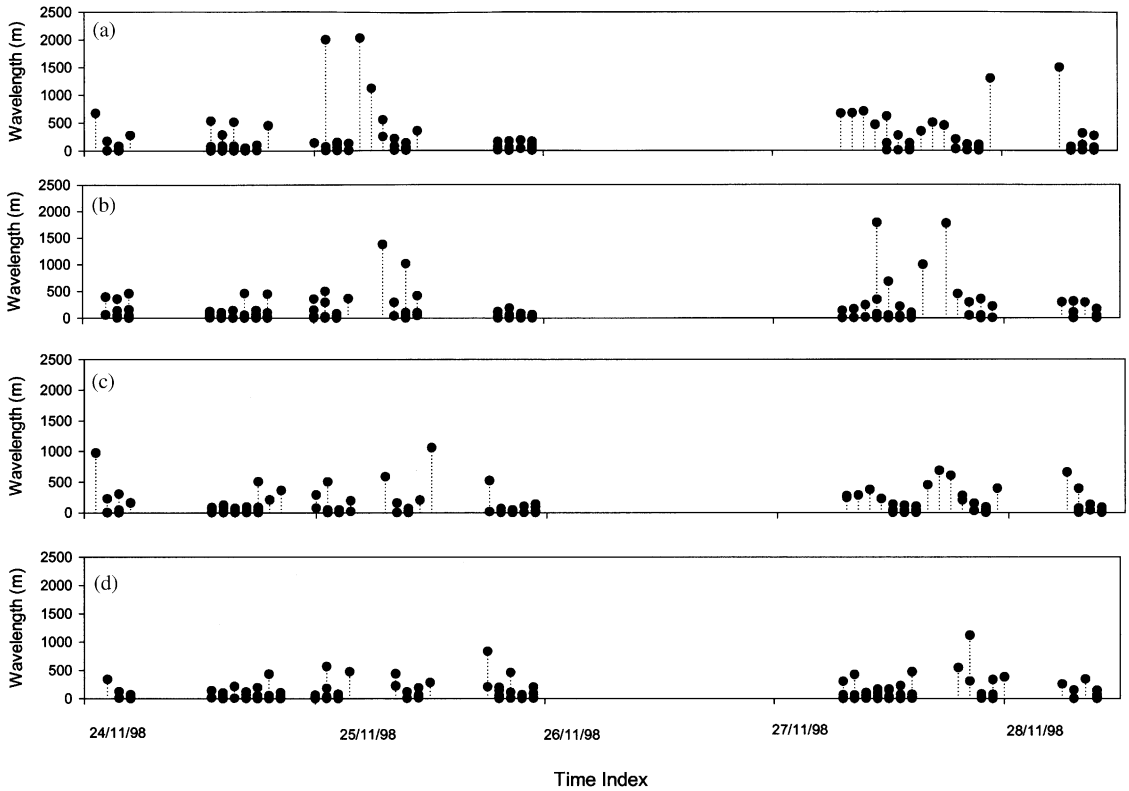

Fig. 10. Solutions for Case 3a and 3b: (a) resonant wavelengths first case of 3a; (b) resonant wavelengths second case of 3a ; (c) resonant wavelengths first case of 3b; (d) resonant wavelengths second case of 3b. Dates from 07:00h 24/11/1998 to 01:00h 28/11/1998.

1998, event with weak currents, which were now increased by −0.20 m/s. This is quite reasonable because the driving force for the intensification of the flow on the topography became greater and the resonant events were partially slowed down, which increased the time for their development. When the barotropic flow is directed towards the Mediterranean (+0.20 m/s), the driving force is diminished (Fig. 10b), and there is no resonance activity in the lower layer.

6.2.2. Case 2b: the case of maximal exchange

The conditions of the experiment were the same as in case 1b, but the barotropic current was included assuming Bryden's criterion. Currents of −0.20 m/s (Fig. 10c) and 0.20 m/s (Fig. 10d) were added to the currents at all depths. The tidal current prediction was the same as before.

Now the internal resonant activity became more intense. The resonant wavelengths were equal to 850 m. There are two cases when waves with wavelengths of 4500 and 3000 m appear, however the first one does not match with the values from Table 2. Because it does not match the *topographic criterion of existence*, it must be discarded. As before, the conclusion that lee waves do not appear at maximal water mass exchange is verified.

7. Final remarks

We have studied the influence of the tidal hydrodynamics on the generation of internal lee waves at the Strait of Gibraltar. The keystone of the linear prediction model is the parameterization

of the vertical profiles of the background horizontal velocity and density for the building of the potential function and solving the Taylor–Goldstein equation. The output is the wavelengths of the internal lee waves. We have analyzed several cases and the two main conclusions are: (a) the difference in depth between the interface and the maximum shear locations plays a very important role. Even the inhibition of the internal lee waves is possible. The occurrence of the internal lee waves is an indicator of maximal exchange at the Strait of Gibraltar; (b) subinertial contributions have a significant role because of the alterations of the resonant conditions changing the vertical profile of the horizontal background velocity.

Finally, although the model is linear, it predicts the events recorded in the survey. Hence it will be necessary to include the non-linear terms and to study their role. Also, a more detailed study of the influence of the subinertial time scale phenomena on the generation of lee waves it is necessary. Both problems will guide future studies.

Acknowledgements

The survey was carried out in November 1998 under an agreement between the Departamento de Física Aplicada de la Universidad de Cádiz (UCA) and the Sociedad para la Comunicación fija a través del estrecho de Gibraltar (SECEGSA). The authors are grateful to Mr. J. Izquierdo and Mr. M. Esteras (SECEGSA) for providing the bathymetric profiles. Dr. F. Ortegón and Dr. A. Ruiz Cañavate (UCA) for providing some bibliographic references, and to Dr. Paul Sacks (Iowa State University) for his suggestions in solving the Sturmian problem. We are grateful to Dr G. Parrilla (Instituto Español de Oceanografía) and to the other, anonymous, reviewer for their very useful comments, patient reading and suggestions that improved the original manuscript and finally to Mr Robert Mason from NEMOC Rota Base (Cádiz) for his suggestions. This work was partially supported by the MAR 99-0643-C03-01 CICYT project and REN2001-2733-C02-01/MAR.

References

Alonso, J.J., Bruno, M., Mañanes, R., Tejedor, L., 1994. Análisis espectral de máxima entropía. Boletín del Real Observatorio de Armada No 5/94.

Armi, L., Farmer, D.M., 1988. The flow of Mediterranean water through the Strait of Gibraltar. Progress in Oceanography 21, 1–105.

Bailey, P.B., Garbow, B.S., Kaper, H.G., Zetti, A., 1991. Transactions on Mathematical Software 17N (4), 500–501.

Bogucki, D., Redekopp, L.G., Dickey, T., 1999. Sediment resuspension and mixing by resonantly generated internal solitary waves. Journal of Physical Oceanography 27, 1181–1196.

Brandt, P., Alpers, W., Backhaus, J.O., 1996. Study of the generation and propagation of the internal waves in the Strait of Gibraltar using a numerical model and synthetic aperture radar images of the European ERS-a satellite. Journal of Geophysical Research 101, 14252–14327.

Bray, N.A., Winant, C.D., Kinder, T.H., Candela, J., 1990. Generation and kinematics of the internal tide in the Strait of Gibraltar, The Physical Oceanography of Sea Straits. In: Pratt, L. (Ed.), NATO Asi. Series C: Mathematical and Physical Sciences, 318, Kluwer Academic Publishers, Dordrecht, pp. 477–491.

Bruno, M., Mañanes, R., Alonso, J., Tejedor, L., Kagan, B., 2000. Vertical structure of the semidiurnal tidal currents at Camarinal Sill, the Strait of Gibraltar. Oceanologica Acta 23 (1), 15–24.

Bruno, M., Alonso, J., Cózar, A., Vidal, J., Echevarría, F., Ruiz, J., Ruiz, A., 2002. The boiling water phenomena at Camarinal Sill, the Strait of Gibraltar. Deep-Sea Research II 49, 4097–4113.

Bryden, H., (2000). Monitoring of water exchange at the Gibraltar Sill, II. In: Alonso, J.J., Ortegón, F. (Eds.), Workshop on Variables Analysis and Numerical Simulation of Water Masses Exchange through the Strait of Gibraltar, Cádiz, June, 28–30.

Bryden, H., Candela, J., Kinder, T., 1994. Exchange through the Strait of Gibraltar. Progress in Oceanography 33, 201–248.

CANIGO, 1999. Final Scientific Report, MAST III, CT96-0060.

Cavanie, A.G., 1972. Observations de fronts internes dans le detroit de Gibraltar pendant la Campagne océanographique OTAN 1970 et interpretation des résultats par un modéle mathématique. Mémories de la Societé des Sciences de Liége 6, 27–41.

Chandrasekar, S., 1981. Hydrodynamic and Hydromagnetic Stability. Dover Publication, New York.

Echevarría, F., Gómez, F., García Lafuente, J., Gorsky, G., Goutx, M., González, N., Bruno, M., García, C., Vargas, J.M., Picheral, M., Striby, L., Alonso del Rosario, J., Reul, A., Cózar, A., Prieto, L., Jiménez-Gómez, F., Varela, M., 2002. Physical–biological coupling in the Strait of Gibraltar. Deep-Sea Research II 49, 4115–4130.

Farmer, D., Armi, L., 1999. The generation and trapping of solitary waves over topography. Science 283, 188–190.

Foreman, M.G.G., 1998. Manual for Tidal Heights and Prediction. Institute of Ocean Sciences, Victoria Bay Institute, Canada.

Frassetto, R., 1964. Short period vertical displacements of the upper layers in the Strait of Gibraltar. Technical Report 30, SACLANT ASW, Res. Center, La Spezia, Italy.

Garrett, C.J.R., Munk, W.H., 1972. Space-time scales of internal waves. Geophysics and Fluid Dynamics 3, 225–264.

Gill, A.E., 1982. In: Donn, W.L. (Ed.), Atmosphere-Ocean Dynamics, International Geophysics Series. Academic Press, New York.

Henrici, P., 1962. Discrete Variable Methods in Ordinary Differential Equations. Wiley, New York.

Konyaev, K.V., Sabinin, K.D., 1992. Waves inside the Ocean. Gidrometeoizdat (in Russian), p. 271.

Kundu, P.J., 1990. Fluid Mechanics. Academic Press, New York.

Lacombe, H., Richez, C., 1984. Hydrography and currents in the Strait of Gibraltar. Office of Naval Research, Sea Straits Report 3, NORDA.

La Violette, P.E., Lacombe, H., 1988. Tidal induced pulses in the flow through the Strait of Gibraltar. Oceanological Acta SP, 13–17.

La Violette, P.E., Kinder, T.H., Green, D.W., 1986. Measurement of internal wave in the Strait of Gibraltar using shore based radar. Technical Report 118, Naval Ocean Research and Development Activity, National Space Technology Laboratory, Bay of St. Louis, MI, 13pp.

Marple, S.L., 1987. Digital Spectral Analysis with Applications. Prentice-Hall, Englewood Cliffs, NJ.

New, A., Pingree, R.D., 1992. Local generation of internal soliton packets in the central Bay of Biscay. Deep Sea Research 39, 1521–1534.

Press, W.H., Flannery, B.P., Teukolsky, S.A., Vetterling, W.T., 1986. Numerical Recipes. Cambridge University Press, Cambridge.

Purdy, J., 1840. The New Sailing Directory for the Strait of Gibraltar and the Western Division of the Mediterranean Sea. HMSO, London.

Richez, C., 1994. Airbone synthetic aperture radar tracking of internal waves in the Strait of Gibraltar. Progress in Oceanography 33, 93–159.

Tofiño, V., 1832. Derrotero de las costas de España en el Mediterráneo y su correspondiente de África. Dirección de Hidrografía. Instituto Hidrográfico de la Marina.

Watson, G., Robinson, L.S., 1990. A study on internal wave propagation in the Strait of Gibraltar using shore-based radar images. Journal of Physical Oceanography 20, 374–395.

Ziegenbein, J., 1969. Short internal waves in the Strait of Gibraltar. Deep Sea Research 16, 479–487.